# Ion velocity and plasma potential measurements of a cylindrical cusped field thruster

Cite as: J. Appl. Phys. **111**, 093303 (2012); https://doi.org/10.1063/1.4707953
Submitted: 14 October 2011 . Accepted: 29 March 2012 . Published Online: 07 May 2012

N. A. MacDonald, C. V. Young, M. A. Cappelli, and W. A. Hargus

# Ion velocity and plasma potential measurements of a cylindrical cusped field thruster

N. A. MacDonald,[1,a)] C. V. Young,[1] M. A. Cappelli,[1] and W. A. Hargus, Jr.[2]
[1]*Stanford Plasma Physics Laboratory, Stanford University, Stanford, California 94305, USA*
[2]*Spacecraft Propulsion Branch, Air Force Research Laboratory, Edwards AFB, California 93524, USA*

(Received 14 October 2011; accepted 29 March 2012; published online 7 May 2012)

Measurements of the most probable time-averaged axial ion velocities and plasma potential within the acceleration channel and in the plume of a straight-channeled cylindrical cusped field thruster operating on xenon are presented. Ion velocities for the thruster are derived from laser-induced fluorescence measurements of the $5d[4]_{7/2} - 6p[3]_{5/2}$ xenon ion excited state transition centered at $\lambda = 834.72$ nm. Plasma potential measurements are made using a floating emissive probe with a thoriated-tungsten filament. The thruster is operated in a power matched condition with 300 V applied anode potential for comparison to previous krypton plasma potential measurements, and a low power condition with 150 V applied anode potential. Correlations are seen between the plasma potential drop outside of the thruster and kinetic energy contours of the accelerating ions. © *2012 American Institute of Physics*. [http://dx.doi.org/10.1063/1.4707953]

## I. INTRODUCTION

Growing interest in the satellite community to reduce spacecraft size and cost has created a desire to scale down current plasma propulsion technologies to low power. Hall thrusters are one of the few plasma propulsion devices that have shown promise for accommodating this low power regime. However, several issues arise with Hall thrusters when scaling down in power. Studies[1,2] on Hall thruster scaling have shown that reducing the power of a thruster by a factor of $\zeta$ requires a reduction in wall area by a factor of $\zeta^2$. This results in increased heat flux to the discharge channel walls, especially along the center pole piece characteristic of annular Hall thrusters. Increased insulator erosion caused by this additional heat loading,[1,2] as well as ion sputtering to the discharge chamber walls,[3] has been shown to limit the lifetime of these electric propulsion devices. The development of efficient low-power Hall thrusters is further limited by the lack of understanding of cross-field transport mechanisms which meter the flow of electrons to the anode.

Drawing from experience with Hall thrusters, several novel thruster designs have been developed in the recent years to address these scaling issues. These include the so-called cylindrical Hall thruster (CHT),[4] diverging cusped field thruster (DCFT),[5] and the cylindrical cusped field thruster (CCFT).[6] The CHT design retracts the center pole piece that is common in annular Hall thrusters, leaving a cylindrical channel.[7] This, combined with a potential drop occurring largely outside the discharge channel, reduces the adverse effects of heat loading and erosion caused by high velocity ions impacting the channel walls.[8,9] The CHT has demonstrated anode efficiencies ranging from 20% to 28% when operating on xenon at powers between 100 and 200 W.[10] The DCFT has a conical discharge channel lined with three permanent magnets of alternating polarity. The cusped magnetic field profile diminishes in strength towards the exit plane of the thruster. The magnetic bottles between cusps mitigate electron flow directly to the anode, thereby increasing electron residence time and creating efficient ionization regions. It also minimizes wall interactions due to the primarily axially pointing magnetic field. The DCFT has demonstrated anode efficiencies of around 40% in the 200 W power range.

This paper presents a study of the CCFT operating on xenon. Like the DCFT, the CCFT generates its cusped magnetic field profile by employing a series of permanent magnets of alternating polarity. The magnets have varying strengths, weakening further downstream of the anode to qualitatively reproduce the magnetic field structure seen in the divergent design. However, unlike the DCFT, it employs a straight cylindrical channel. Previous studies[6] have shown that when operating on krypton, the CCFT demonstrated anode efficiencies of around 23% at power levels ranging from 40 to 240 W. The discharge did not exhibit the strong oscillations seen in the DCFT in high current mode.[5] While it is not yet clear how the straight channel configuration of the CCFT affects the discharge dynamics, we suspect that the quiescent nature of the discharge current may be attributed to the higher propellant density resulting from the non-divergent channel. The work presented here seeks to characterize the CCFT operating with the more commonly used xenon propellant and employs laser-induced fluorescence (LIF) from xenon ions to study ion transport in the very near field of the discharge. This measured ion velocity, established as a result of the kinetic acceleration of ions in the imposed electric field, is interpreted in conjunction with plasma potential measurements acquired using an emissive probe.

Time-averaged xenon ion velocities for the thruster are derived from LIF measurements of the $5d[4]_{7/2} - 6p[3]_{5/2}$ xenon ion excited state transition at $\lambda = 834.72$ nm. The measured spectral feature, which is a convolution of the ion velocity distribution function (VDF) and the transition lineshape, is used to determine the most probable axial ion velocities at various positions throughout the thruster channel and the near-field plume. These axial velocities are also

a)Electronic mail: smacdo@stanford.edu.

 

used to determine the axial component to the ions' kinetic energies. Potential measurements are made using a floating emissive probe similar to that used to characterize the near-field of a low-power Hall thruster.[11] The emissive probe consists of a thoriated-tungsten thermionic electron-emitting filament, resistively heated by a direct current until saturation at the local plasma potential. The potential drop measured by the probe is then compared to the increased kinetic energies of the ions.

## II. EXPERIMENT

Figure 1(a) shows a schematic of the CCFT, including the magnetic field topology derived from a finite element method magnetics (FEMM) simulation of the magnetic circuit. During operation, the anode is powered at high positive potential relative to the cathode, which is at ground potential.

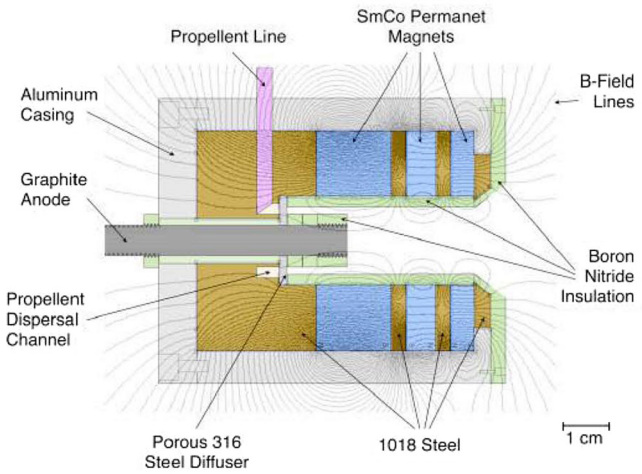


a) CCFT Schematic

b) CCFT Operating on Xenon

FIG. 1. (a) Schematic of CCFT developed by Stanford including magnetic field simulated by FEMM. (b) CCFT operating on xenon propellant under power matched conditions.

The electric field between the anode and cathode (not shown in the figure, but located downstream and off the centerline axis) is established by the resistance to electron migration imposed by the magnetic field—a process that is not yet well understood. Propellant is introduced between the channel and the cylindrical anode at the base of the channel, upstream of a porous steel diffuser. Electrons emitted from the cathode initially migrate along the magnetic field lines, gaining energy from the electric field and colliding occasionally with propellant atoms to produce secondary electrons and avalanche ionization. The newly generated ions are accelerated downstream by the electric field, and because of the relatively large mass, are not strongly affected by the magnetic field. The electrons mirror from regions of magnetic field convergence (cusps) and bounce between these cusps, increasing their residence time in the plasma and enhancing the possibility of further ionization events. Some electrons have enough energy to overcome repulsion from the sheath and scatter off of the channel wall. These electrons may "skip" across the magnetic field, eventually landing on a magnetic field line that allows them to reach either the next cusp, or the anode. The magnetic field lines also converge on the graphite anode located at the base of the channel centered on the main axis. The mirroring of the electrons from this anode region provides a mechanism to restrict the electrons captured by the anode. We anticipate that the overall performance of this thruster will depend on the location of this anode relative to the magnetic topology; however, for the studies described here, the anode location was not varied.

The construction of the thruster channel is relatively simple. The CCFT outer aluminum casing is 7 cm in length with an outer diameter of 6 cm. The cylindrical channel, lined with a boron nitride (BN) sleeve, is 4 cm in length and 1.4 cm in diameter, except for the chamfered edge at the exit plane. This divergent edge ensures that electrons traveling along field lines from the cathode have a path to enter the discharge channel with minimal collisions with the front face of the thruster.[6] The magnetic field profile is generated by three samarium cobalt permanent magnets of alternating polarity and shaped by type 1018 steel spacers. These magnets diminish in strength as they approach the exit plane, creating a divergent magnetic field profile even though the channel is cylindrical.

The thruster is pictured operating on xenon in Fig. 1(b). The photograph in this figure is a side view, with the exit of the cathode facing the direction of observation. Apparent in this figure is a bright, luminous conical region, similar to that seen in the DCFT,[5] indicating that the shape of this luminous plasma is not determined by the divergence of the channel, but rather, the magnetic field topology.

Two operating conditions were examined in this study. The first was chosen to reproduce conditions seen in a previous study,[6] where extensive probe measurements were taken on the CCFT running on krypton propellant at 111 W anode power. In the current study, the thruster was run with xenon propellant, at an applied anode potential of 300 V and propellant flow rate of 147 $\mu$g/s Xe to achieve 111 W of anode power. This condition is summarized in Table I. The second

TABLE I. Power matched operating condition.

| | |
|---|---|
| Anode flow | 690 $\mu$g/s Xe |
| Anode potential | 300 V |
| Anode current | 0.37 A |

operating condition, summarized in Table II, was chosen to highlight the low power capabilities of this thruster, with an operating power of 43.5 W. Both operating conditions were very quiescent, showing no oscillations in anode discharge current.

LIF measurements were performed at the Air Force Research Laboratory (AFRL) at Edwards AFB, CA. The thruster operated in a vacuum facility capable of maintaining a background pressure of $5 \times 10^{-6}$ Torr during thruster operation. A Busek cathode was used as the electron source, with specifications described in Table III. Plasma potential measurements were performed at the Stanford Plasma Physics Laboratory (SPPL) at Stanford University. The background chamber pressure for this facility was $1 \times 10^{-5}$ Torr while operating the thruster. During the tests at Stanford, an Iontech cathode was used, as a Busek cathode was unavailable. The slight differences in cathode operation appear to have little to no effect on the overall thruster behavior (as determined by the thruster operating characteristics); the thruster proved to be invariant to changes in supplied cathode keeper current between 0.25 and 1.3 A. Cathode position has been shown to be more critical to thruster operation,[12] and so the cathode was placed in the same position relative to the cylindrical channel for both sets of tests. The difference in background chamber pressures has been shown in previous work[13,14] to affect ion acceleration, with higher pressures pushing the peaks in acceleration upstream towards the anode. The background chamber effects, and the inherently intrusive nature of emissive probes (as compared to the non-intrusive nature of laser diagnostics), should factor into the comparison of the LIF and plasma potential measurements made here.

The LIF experimental apparatus at AFRL has been described extensively in previous work.[15,16] Axial ion velocity measurements are accomplished by probing the $5d[4]_{7/2} - 6p[3]_{5/2}$ electronic transition of Xe II at 834.72 nm with a tunable external-cavity diode laser (New Focus, Model TLB-6017). The upper state of this transition is shared by the relatively strong $6s[2]_{3/2} - 6p[3]_{5/2}$ transition at 541.92 nm,[17] allowing for non-resonant fluorescence collection. Ion velocities are determined by measuring the Doppler shifted fluorescence excitation spectrum.[18] This particular transition has been used in past studies to characterize a variety of thrusters operating on xenon.[14,15,19,20] Note that only axial ion velocities will be presented in this paper, as radial measurements are ongoing.

TABLE II. Low power operating condition.

| | |
|---|---|
| Anode flow | 690 $\mu$g/s Xe |
| Anode potential | 150 V |
| Anode current | 0.29 A |

TABLE III. Cathode operating conditions.

| Cathode | Cathode flow | Keeper current (A) | Heater current (A) |
|---|---|---|---|
| Busek | 150 $\mu$g/s Xe | 0.5 | 3.0 |
| Iontech | 140 $\mu$g/s Ar | 0.25 | 6.0 |

Emissive probe plasma potential measurements in low power plasma propulsion sources have also been described extensively in previous work.[6,11] The emitting portion of the probe consists of a 2 mm diameter loop of 150 $\mu$m diameter thoriated-tungsten (1%) wire, connected to copper wire encased in a 2.5 mm diameter alumina tube. A direct current of 2.5 A is driven through the probe to heat the thoriated-tungsten filament until its signal is saturated, at which point the probe filament is floating at the potential of the surrounding plasma.

## III. RESULTS AND DISCUSSION

The ion velocities presented here represent the most probable (or peak) values in an axial ion velocity distribution calculated from the Doppler shift in laser fluorescence excitation spectrum relative to the absorption peak recorded in a stationary xenon discharge reference. Contour plots of the most probable axial ion velocities are shown in Fig. 2, where (a) shows the power matched condition and (b) shows the low power condition. $\Delta$ symbols indicate measurement locations. Interpolation around these points is accomplished using an inverse-distance method, given by Eq. (1), where $\varphi_d$ is the velocity at the destination point and $\varphi_s$ is the velocity at each source point. The weighting function, $w_s$, is given by Eq. (2), where D is the distance between the source point and the destination point and E is a weighting factor chosen to be 3.5. This weighting factor gives the majority of influence to directly adjacent data points while providing good smoothing:

$$\varphi_d = \frac{\sum w_s \varphi_s}{\sum w_s}, \tag{1}$$

$$w_s = D^{-E}. \tag{2}$$

This interpolation scheme is representative of the analysis throughout these results. The white region in the lower right hand corner of the plots represents the chamfered edge of the thruster channel, with the exit plane located at $Z = 0$ mm.

For the power matched condition, the ions inside the thruster channel retain a relatively low axial velocity ($\leq 2000$ m/s) along the thruster centerline. Off axis at radial locations greater than $R = 6$ mm, the axial ion velocities increase significantly, especially near the chamfered edge of the thruster, which contains the outermost (third) magnetic cusp. As seen in Fig. 1(a), this third magnetic cusp intersects the center of the chamfered edge, defining a separatrix which appears to form a boundary between an ionization region characterized by low ion velocity and a region of strong axial ion acceleration. Therefore, it appears that there is a close relation between the separatrix and the plasma potential. Downstream of the separatrix, the ions reach a maximum

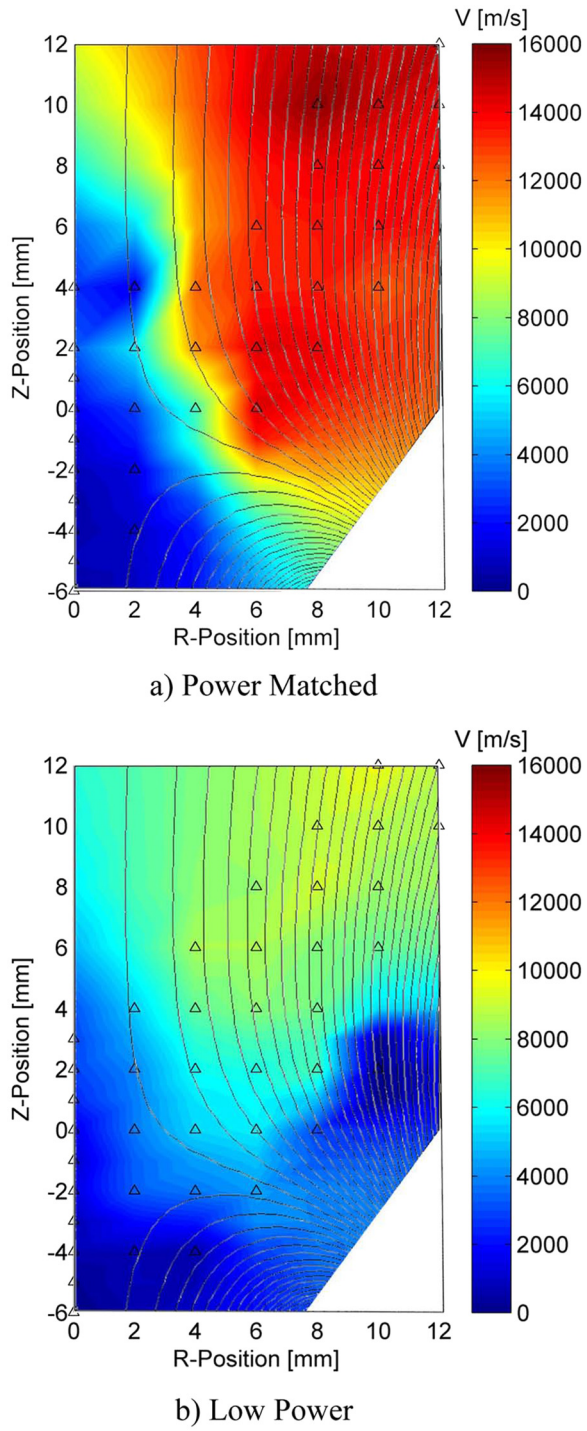


FIG. 2. Most probable axial ion velocities for CCFT operating under (a) power matched and (b) low power operating conditions. Δ symbols indicate measurement locations.

axial velocity of 15 600 m/s at $Z = 10$ mm, $R = 8$ mm. In general, the ions with higher axial velocities appear away from the centerline, in the region corresponding to the visibly luminous conical plume observed in Fig. 1(b).

The low power operating condition shows similar trends in the contour plot of axial ion velocity, with the overall magnitudes being expectedly lower due to the lower applied anode potential (150 V vs. 300 V for the power matched condition). The lower velocity ions reside closer to the centerline inside the thruster, while higher velocity ions (reaching 9600 m/s axial velocity) appear farther into the plume at $R > 8$ mm. In this case, the boundary of the acceleration region does not appear to be as directly related to the separatrix near the exit plane of the thruster. This indicates that the particular discharge operating conditions influence how the magnetic topology and plasma potential are interconnected.

We also find that the region of low axial ion velocity along the centerline does not extend as far into the plume. Rather, acceleration appears to occur at all radii across the exit plane between $Z = 2$ mm and $Z = 6$ mm. For example, the power matched condition has a peak axial ion velocity of 15 600 m/s and a maximum axial velocity of 9400 m/s along the centerline, whereas the centerline axial velocity for the low power condition peaked at 6500 m/s, which is more comparable in magnitude to the 9600 m/s seen away from the centerline. When operating in the low power mode, the luminous region is visibly less bright the power matched condition, and is distributed throughout the center of the plume instead of just the outer conical region. This could be attributed, in part, to a more even distribution of ions moving throughout the plume with lower average velocity.

Figure 3 shows emissive probe measurements of the plasma potential, $\phi_p$, for both operating conditions. Probe data were taken in a horizontal plane passing through the center of the thruster exit plane and cathode, excluding area occupied by the cathode and a bolt on the exterior face of the thruster. For the power matched condition, the maximum plasma potential measured in the plume was 37 V at the edges of the discharge channel wall near the exit plane of the thruster ($Z = 0$ mm, $R = \pm 10$ mm). By 20 mm into the plume, the plasma potential drops to around 20 V, except for a conical jet of higher potential at an angle of 35° from the main axis, which remains as high as 30 V by 20 mm into the plume. The jet is asymmetric, being interrupted on the cathode side by a region of lower potential (≈10 V). The region of elevated plasma potential corresponds visually with the luminous conical jet seen in Fig. 1(b). When operating on krypton, this region also correlated with the highest ion current density.[6]

For the low power condition, the maximum plasma potential measured was higher than the power matched condition: 46 V at the exit plane of the thruster along the centerline ($Z = 0$ mm, $R = 0$ mm). The potential profile also displays a somewhat conical shape in the regions of higher potential; however, the potential also remains elevated throughout the center of the cone (upwards of ≈ 35 V on the cathode side). Once again, this corresponds to the distribution of luminous regions observed throughout the conical plume. Of note when comparing the two operating conditions, the power matched case has a larger potential drop inside the thruster channel (300 V to less than 50 V at the exit plane), whereas the low power case has a potential drop that is more distributed throughout the plume (only 150 V to ≈60 V at the exit plane). With the bulk of the plume remaining at a 25–35 V plasma potential, the low power condition appears to be less efficient at converting applied anode potential to ion acceleration.

Figure 4 gives a close-up of the plasma potential measurements, including points inside the discharge channel, with

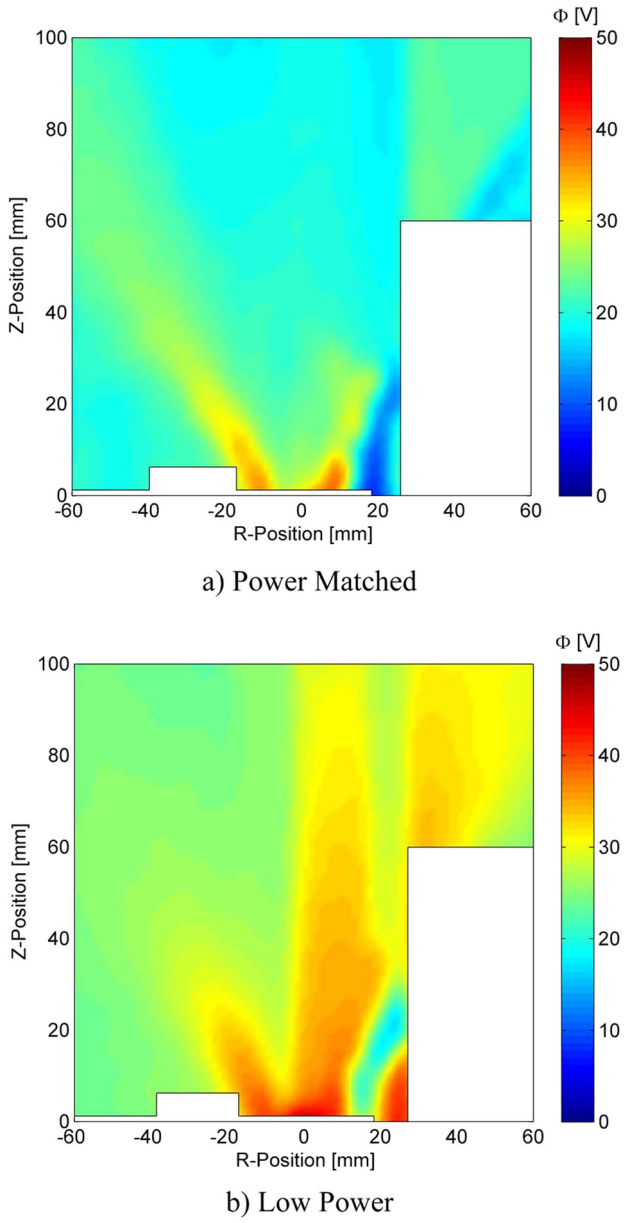


FIG. 3. Plasma potential measurements in the near-field CCFT plume operating under (a) power matched and (b) low power operating conditions.

overlaid contours of the axial kinetic energy profiles derived from LIF measurements of axial ion velocity. Radial LIF measurements were not taken in this experiment; therefore, the kinetic energy contours should not be taken as an overall magnitude. For the power matched condition, Fig. 4(a) shows that there is a large drop in potential between $Z = -6$ mm inside the thruster channel and the exit plane at $R > 7$ mm (i.e., the radius at the edge of the cylindrical portion of the thruster channel). The border between high and low potential follows a portion of the kinetic energy contour that delimits ≈20 eV ions. However, this 20 eV region extends 8 mm into the plume, while the potential drop appears contained within the thruster. The plasma potential remains relatively constant ≈30 V outside the thruster. This appears not to match the gradient seen in the kinetic energy contours, where ions gain energy from 20 eV to 160 eV by 12 mm into the plume.

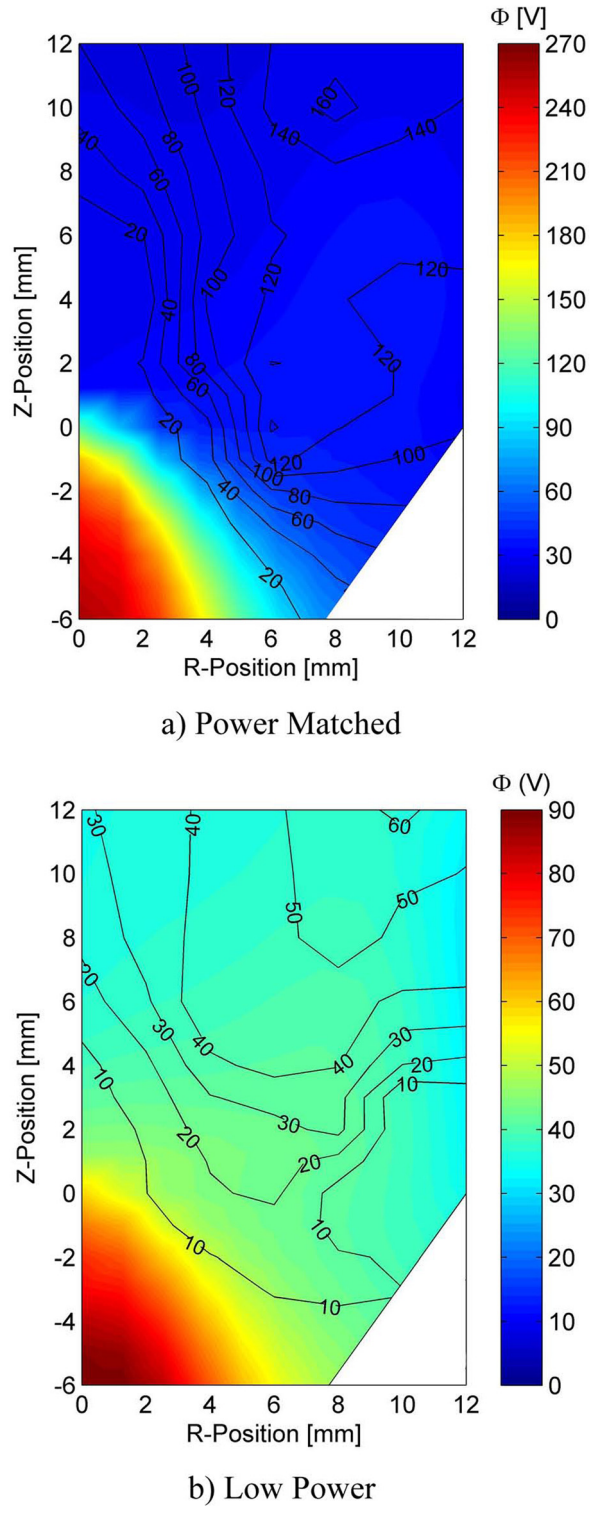


FIG. 4. Close up of plasma potential with kinetic energy contour overlay for the CCFT plume operating under (a) power matched and (b) low power operating conditions.

Qualitatively, the low power plasma potential map seen in Fig. 4(b) is very similar to the power matched condition, exhibiting a large potential drop just inside the thruster exit plane followed by a relatively constant potential out to 12 mm. The potential drop inside the thruster is less severe for the low power condition, only decreasing from 90 V to 40 V, compared to the 230 V drop seen in the power matched

condition. The lowest kinetic energy contour (this time 10 eV) more closely matches the potential drop; however, the gain in axial kinetic energy outside the exit plane is unmatched by any further potential drop.

Figure 5 shows the plasma potential and ion kinetic energies along the centerline of the thruster for both the power matched and low power operating conditions. Radial velocities along the centerline of the thruster are assumed to be approximately zero, due to the symmetry of the discharge. This figure better illuminates the differences between the LIF and probe measurements, as well as those between the two operating conditions. The sharp potential drop seen near the exit plane for the power matched condition is more gradual for the low power case. For both conditions, the majority of the gain in axial ion kinetic energy does not occur until approximately 5 mm outside of the thruster, at which point the plasma potential has already flattened out to a nearly constant value.

The differences between the plasma potential maps and LIF derived kinetic energies could have several causes. As mentioned above, the difference in background pressure at the two facilities could slightly shift the regions of ion acceleration corresponding to the drop in potential. The SPPL chamber background pressure was approximately twice that of the AFRL chamber, likely resulting in the potential drop and peak ion acceleration being pushed upstream. Additionally, emissive probes are inherently intrusive by nature, with the potential to alter the operation of the thruster, especially when taking measurements inside the thruster channel. Therefore, when comparing measurements from the different facilities, differences should be expected—especially near the exit plane of the thruster.

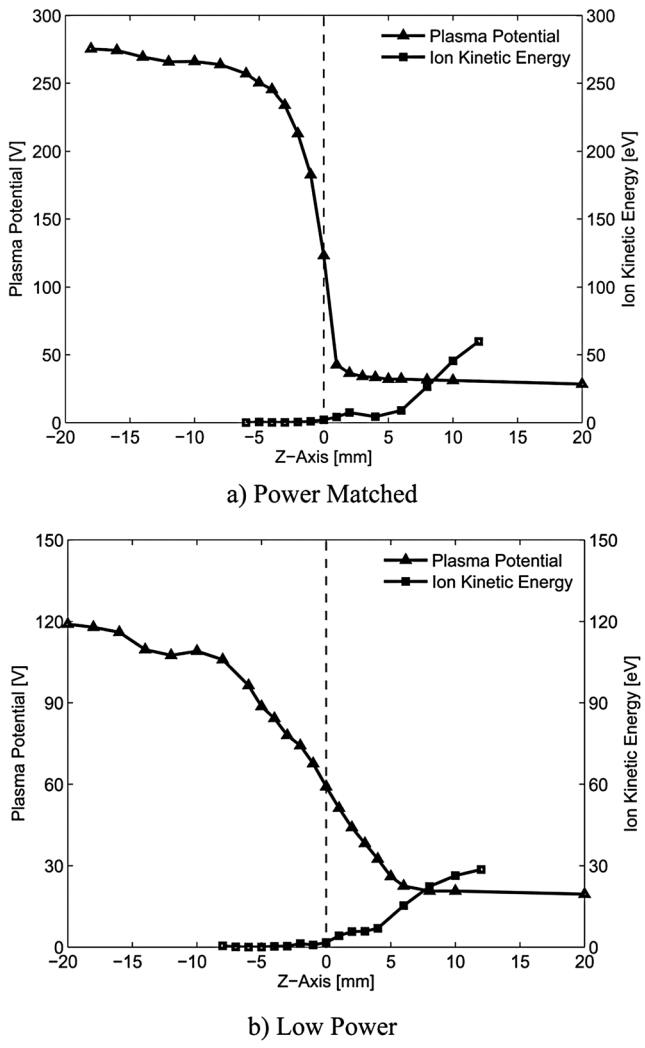


FIG. 5. Plasma potential and axial ion kinetic energy measurements along the centerline of the CCFT operating under (a) power matched and (b) low power operating conditions.

## IV. CONCLUSIONS

Laser induced fluorescence velocimetry and emissive probe plasma potential measurements were used to characterize the Stanford University Cylindrical Cusped Field Thruster operating on xenon. Two operating conditions were considered, including a condition that was power matched to a previous study[6] running on krypton propellant, and a low power operating condition that reduced the supplied anode potential of the power matched case by half. Contour plots of the most probable axial ion velocities revealed several trends: low velocity ions resided inside the thruster channel away from the walls, extending along the centerline into the plume, and a conical jet of ions exhibited higher axial velocity outside the separatrix formed by the third magnetic cusp. Plasma potential measurements also suggested a conical profile, which was asymmetric due to the influence of the cathode for both conditions. The low power case had a higher plasma potential distributed throughout the plume than the power matched condition, which mainly showed high potential in the conical jet regions.

Comparisons between the plasma potential and LIF-derived kinetic energies revealed that for both operating conditions, the majority of the potential drop occurred inside the thruster channel while a significant gain in axial kinetic energy was attained just outside the exit plane. These differences are mainly attributed to the intrusive nature of probes altering the operation of the thruster, and the elevated background chamber pressure seen at SPPL causing the potential drop (and thereby the acceleration region) to be moved upstream into the thruster channel. Overall, the power matched condition appeared to more effectively convert the applied anode potential into axial ion kinetic energy.

## ACKNOWLEDGMENTS

The authors would like to thank A. Smith of Stanford University and B. Gregory, Lt. A. Campos, and G. Arzonia of AFRL for their technical support. N. A. MacDonald acknowledges the Science Mathematics and Research for Transformation (SMART) scholarship program for support of her research. C. V. Young acknowledges support from the U.S. Department of Energy Stewardship Science Graduate Fellowship (SSGF) provided under Grant No. DE-FC52-08NA28752. Research at Stanford is funded through the Air Force Office of Scientific Research with Dr. M. Birkan as grant monitor.

[1]V. Khayms and M. Martinez-Sanchez, in *Proceedings of the 32nd AIAA, ASME, SAE, and ASEE, Joint Propulsion Conference and Exhibit on Design of a Miniaturized Hall Thruster for Microsatellites, Lake Buena Vista, FL, 1-3 July 1996* (American Institute of Aeronautics and Astronautics, 1996), AIAA Paper No. 96-3291.
[2]D. P. Schmidt, N. B. Meezan, W. A. Hargus, Jr., and M. A. Cappelli, Plasma Sources Sci. Technol. **9**, 68 (2000).
[3]V. Kim, "Stationary plasma thrusters," J. Propul. Power **14**, 736 (1998).
[4]Y. Raitses and N. J. Fisch, Phys. Plasmas **8**, 2579 (2001).
[5]D. G. Courtney and M. Martinez-Sanchez, in *Proceedings of the 30th International Electric Propulsion Conference on Diverging Cusped-Field Hall Thruster (DCHT), Florence, Italy, 17-20 September 2007* (Electric Rocket Propulsion Society, 2007), IEPC Paper No. 2007-39.
[6]C. V. Young, A. W. Smith, and M. A. Cappelli, in *Proceedings of the 31st International Electric Propulsion Conference on Preliminary Characterization of a Diverging Cusped Field (DCF) Thruster, Ann Arbor, MI, 20-24 September 2009* (Electric Rocket Propulsion Society, 2009), IEPC Paper No. 2009-166.
[7]Y. Raitses, E. Granstedt, A. Smirnov, E. Merino, and N. J. Fisch, in *Proceedings of the 44th AIAA/ASME/SAE/ASEE Joint Propulsion Conference & Exhibit on Effects of Cathode Electron Emission on Hall Thruster Discharge, Hartford, CT, 21-23 July 2008* (American Institute of Aeronautics and Astronautics, 2008), AIAA Paper 2008-5288.
[8]Y. Raitses, A. Smirnov, and N. J. Fisch, in *Proceedings of the 37th AIAA Plasmadynamics and Lasers Conference on Cylindrical Hall Thrusters, San Francisco, CA, 5-8 June 2006* (American Institute of Aeronautics and Astronautics, 2006), AIAA Paper 2006-3245.
[9]A. Smirnov, Y. Raitses, and N. J. Fisch, J. Appl. Phys. **95**, 2283 (2004).
[10]A. Smirnov, Y. Raitses, and N. J. Fisch, Phys. Plasmas **14**, 057106 (2007).
[11]A. W. Smith and M. A. Cappelli, "Field of a coaxial Hall plasma discharge," Phys. Plasmas **16**, 073504 (2009).
[12]C. V. Young, "The Stanford diverging cusped field thruster: Design, construction, and initial testing," Honors Thesis (Stanford University, 2010).
[13]M. R. Nakles and W. A. Hargus, Jr., in *Proceedings of the 44th AIAA/ASME/SAE/ASEE Joint Propulsion Conference & Exhibit on Background Pressure Effects on Internal and Near-field Ion Velocity Distribution of the BHT-600 Hall Thruster, Hartford, CT, 21-23 July 2008* (American Institute of Aeronautics and Astronautics, 1996), AIAA Paper 2008-5101.
[14]N. A. MacDonald, M. A. Cappelli, and W. A. Hargus, Jr., in *Proceedings of the 31st International Electric Propulsion Conference on Laser-Induced Fluorescence Velocity Measurements of a Low Power Cylindrical Hall Thruster, Ann Arbor, MI, 20-24 September 2009* (Electric Rocket Propulsion Society, 2009), IEPC Paper No. 2009-34.
[15]W. A. Hargus, Jr., and M. R. Nakles, "Low-power Hall thruster," IEEE Trans. Plasma Sci. **36**, 1989 (2008).
[16]W. A. Hargus, Jr., and C. S. Charles, J. Propul. Power **24**, 127 (2008).
[17]J. E. Hansen and W. Persson, Phys. Scr. **4**, 602 (1987).
[18]W. Demtroeder, *Laser Spectroscopy: Basic Concepts and Instrumentation* (Springer-Verlag, Berlin, 1996).
[19]D. H. Manzella, in *Proceedings of the 30th Joint Propulsion Conference and Exhibit on Stationary Plasma Thruster Ion Velocity Distribution, Indianapolis, IN, 27-29 June 1994* (American Institute of Aeronautics and Astronautics, 1994), AIAA Paper No. 94-3141.
[20]S. Mazouffre, D. Gawron, V. Kulaev, and N. Sadehgi, IEEE Trans. Plasma Sci. **36**, 1967 (2008).